NOTES AND CORRESPONDENCE

A Kinematic Analysis of Frontogenesis Associated with a Nondivergent Vortex

CHARLES A. DOSWELL III

National Oceanic and Atmospheric Administration, Environmental Research Laboratories, Weather Research Program, Boulder, CO 80303

18 July 1983 and 22 November 1983

ABSTRACT

An idealized model of a vortex interacting with an initially straight frontal zone is developed. The nondivergent vortex flow is a smoothly varying analog to a Rankine Combined Vortex. Local advection and frontogenesis are calculated analytically at the initial time and used to approximate the temporal evolution of the system, during its early phases. Intuition suggests that the maximum deformation of the frontal zone should occur near the radius of maximum winds. Results confirm our intuition, but also provide insights into how frontogenesis proceeds in a real vortex. The calculations yield patterns surprisingly similar to observations of vortex interactions with zones of high gradient on several scales, and seem to explain the compelling similarities between observed vortex phenomena on widely different scales.

1. Introduction

The classical kinematic approach to frontogenesis follows the work of Miller (1948) or Petterssen (1956). The definition of frontogenesis they give is

$$F = (d/dt)|\nabla Q|, \tag{1}$$

where the operator d/dt *follows the air parcels* and where $Q = Q(x, y, z, t)$ is any quantity—say potential temperature. The operator d/dt is further defined for the general variable Q to be

$$\frac{dQ}{dt} = \frac{\partial Q}{\partial t} + \mathbf{V}\cdot\nabla Q + w\frac{\partial Q}{\partial z}, \tag{2}$$

where $\mathbf{V}$ is the horizontal velocity of the flow, ∇ is the horizontal del operator, and w is the vertical flow component.

Strictly speaking, we are probably most interested in the frontal gradient *following the front*, rather than the air. Nevertheless, frontogenesis is considered here to be defined by (1). Such an expression is perhaps most appropriate whenever Q is a conservative quantity (i.e., $dQ/dt \equiv 0$). It is straightforward to show from (1) and (2) that

$$F = \mathbf{e}_F\cdot\left[\nabla\left(\frac{dQ}{dt}\right) - (\nabla Q\cdot\nabla)\mathbf{V} - \frac{\partial Q}{\partial z}\nabla w\right], \tag{3}$$

where $\mathbf{e}_F$ is a unit vector in the direction of ∇Q—i.e., $\mathbf{e}_F \equiv |\nabla Q|^{-1}\nabla Q$. The first term in (3) within the brackets is the contribution to changes in parcel Q by nonconservative effects (e.g., diabatic effects if Q is the potential temperature), the second represents the combined influences of divergence and deformation in the direction of the frontal gradient and the third is the change of horizontal gradients by tilting of *vertical* gradients resulting from horizontal variations in vertical velocity.

For a purely horizontal flow, with Q absolutely conserved, (3) reduces to

$$F = \mathbf{e}_F\cdot[-(\nabla Q\cdot\nabla)\mathbf{V}]. \tag{4}$$

Thus, under these somewhat restrictive conditions, frontogenesis is accomplished purely by divergence and deformation. It is common to write (4) in terms of the kinematic properties of the flow—i.e.,

$$F = -\frac{|\nabla Q|}{2}(\mathrm{div} - \mathrm{def}_R\cos 2\gamma). \tag{5}$$

where $|\nabla Q|$ is the magnitude of the horizontal Q gradient, div is the horizontal divergence, def_R is the resultant deformation (see Saucier, 1955, p. 355ff), and γ is the angle between the isopleths of Q and the resultant deformation's axis of dilatation.

Note that the vorticity does not appear in (5) [or in (3), for that matter], which is usually explained by noting that a field of pure rotation does not affect the gradient but, rather, merely rotates it. This and related concepts are examined in what is to follow. The approach taken is purely kinematic, so there is no scale dependence, and the analysis applies equally well to any systems that satisfy the assumptions, be they turbulent eddies, mesoscale vortices, or extratropical cyclones. The approach taken is also analytic, rather than numerical, in order to avoid the problems and complicating issues of differencing schemes, numerical diffusion, spatial truncation, etc. Insights gained by this method would be lost or obscured in a numerical simulation, and even more so if the simulation accounted for dynamics (e.g., Welander, 1955) although insights

about other aspects might well be obtained in such a simulation.

2. Kinematic properties of an idealized vortex

First, consider the four conventional kinematic properties (vorticity, divergence, stretching and shearing deformation). They are derived from the *linear* properties of the wind field. That is, consider the Taylor series expansion of the wind components at the point $x = x_0 + \Delta x$, $y = y_0 + \Delta y$,

$$u(x, y) = u_0 + \frac{\partial u}{\partial x}\Delta x + \frac{\partial u}{\partial y}\Delta y + \frac{\partial^2 u}{\partial x^2}\Delta x^2 + 2\frac{\partial^2 u}{\partial x \partial y}\Delta x \Delta y + \frac{\partial^2 u}{\partial y^2}\Delta y^2 + \cdots, \quad (6a)$$

$$v(x, y) = v_0 + \frac{\partial v}{\partial x}\Delta x + \frac{\partial v}{\partial y}\Delta y + \frac{\partial^2 v}{\partial x^2}\Delta x^2 + 2\frac{\partial^2 v}{\partial x \partial y}\Delta x \Delta y + \frac{\partial^2 v}{\partial y^2}\Delta y^2 + \cdots, \quad (6b)$$

where $u_0 = u(x_0, y_0)$ and $v_0 = v(x_0, y_0)$. Second order (or higher) terms can be neglected when first order terms are roughly an order of magnitude (or more) larger than those of higher order. Thus, nonlinear terms from (6) that satisfy inequalities like

$$\frac{(\partial u/\partial x)\Delta x}{(\partial^2 u/\partial x^2)\Delta x^2} \geq 10, \quad (7)$$

can be ignored. If conventional scaling approaches are employed—i.e.,

$$\frac{\partial u}{\partial x} \sim \frac{V}{L}, \quad \frac{\partial^2 u}{\partial x^2} \sim \frac{V}{L^2},$$

where V is a velocity scale and L is a length scale, then (7) becomes

$$\Delta x \leq L/10. \quad (8)$$

Thus, (6) and (8) imply that attention must be restricted to a *neighborhood of a point* within a distance one-tenth of a scaling length from that point, if the neglect of the higher-order properties of the flow field is to be valid.

Formally, this represents no real problem. We simply compute the kinematic properties at a point—implicitly using the linear approximation—and any large scale nonlinear properties of the flow are accounted for by the point-to-point variation. Since frontogenesis is computed in this fashion, it is clear that vorticity can have no effect. The vorticity is *constant within the point's neighborhood,* so it can have no *local* influence on the frontal gradient. However, it is equally obvious that this assumption cannot be extended to larger domains. Vorticity does not remain constant over any realistic field (including our idealized vortex), which means that "globally" the nonlinear nature of the wind field eventually must play a role.

In order to illustrate the situation, consider an idealized pattern of flow and Q-isopleths for which analytic solutions can be obtained. The wind field is taken to be a steady state, two-dimensional, nondivergent vortex with a purely tangential wind (V_T) field which depends only on radius (r) from the origin according to

$$V_T(r) = \operatorname{sech}^2 r \tanh r. \quad (9)$$

This field has been nondimensionalized via division by a characteristic amplitude for the variation of V_T. The flow field and its properties as a function of radius are shown in Fig. 1. A plan view of the initial conditions is revealed by Fig. 2. Note that the x and y components of the flow are, respectively,

$$u(x, y) = -V_T(r)\sin\theta, \quad (10a)$$

$$v(x, y) = +V_T(r)\cos\theta, \quad (10b)$$

where $\theta = \tan^{-1}(y/x)$ and $r = (x^2 + y^2)^{1/2}$. Differentiating (9) and (10) appropriately, it can be shown easily that the divergence is, indeed, zero. This vortex can be thought of as a *smoothly varying* (i.e., one with continuous derivatives) analogue to the Rankine Combined Vortex. Further, it can be shown that

$$\frac{\partial v}{\partial x} - \frac{\partial u}{\partial y} = \operatorname{sech}^2 r\left[\operatorname{sech}^2 r - 2\tanh^2 r + \frac{\tanh r}{r}\right], \quad (11a)$$

$$\frac{\partial u}{\partial x} - \frac{\partial v}{\partial y} = \operatorname{sech}^2 r\left[2\tanh^2 r - \operatorname{sech}^2 r + \frac{\tanh r}{r}\right]\sin(2\theta), \quad (11b)$$

$$\frac{\partial v}{\partial x} + \frac{\partial u}{\partial y} = \operatorname{sech}^2 r\left[\operatorname{sech}^2 r - 2\tanh^2 r - \frac{\tanh r}{r}\right]\cos(2\theta). \quad (11c)$$

The vorticity calculated from (11a) is shown in Fig. 1, as is the magnitude of the resultant deformation—having combined (11b) and (11c) to show that

$$\mathrm{def}_R = \operatorname{sech}^2 r\left|\left[2\tanh^2 r - \operatorname{sech}^2 r + \frac{\tanh r}{r}\right]\right|. \quad (12)$$

If the methods of Saucier are used, the angle of inclination between the x-axis and the *resultant* deformation's axis of dilatation is given by

$$\tan(2\beta) = \frac{(\partial v/\partial x + \partial u/\partial y)}{(\partial u/\partial x - \partial v/\partial y)}. \quad (13)$$

Substitution of (11b) and (11c) into (13) gives

$$\tan(2\beta) = -\frac{\cos(2\theta)}{\sin(2\theta)} = -\cot(2\theta), \quad (14)$$

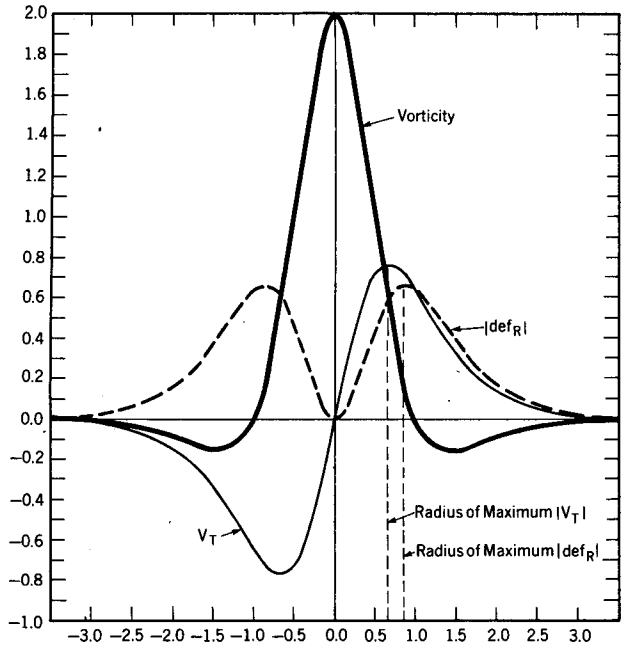

FIG. 1. Radial structure of idealized vortex flow, showing the tangential wind profile (thin solid line), the magnitude of the resultant deformation (dashed line), and the vorticity (thick solid line) as functions of radius. All variables are nondimensional.

or, simply, $\beta = \theta - \pi/4$. These are shown on Fig. 2 at 45° intervals around the circle of maximum tangential wind.

It is worthwhile to note that one can describe the wind field (i.e., its *linear* variation) using vorticity, divergence and the two deformations. However, if the flow is a purely nondivergent vortex, it is straightforward to show (Doswell, 1982) that neither deformation can vanish everywhere in the field unless the entire field is in solid body rotation. Thus, the proposed field of nondivergent vorticity (which varies from point to point) must contain areas of frontogenesis. Intuitively, if the vorticity varies spatially, then any pre-existing gradients are rotated at different rates—resulting in deformations which, in turn, result in frontogenesis. Apart from this, even pure (solid body) rotation, when added to a field of pure deformation, can influence frontogenesis by rotating a scalar field into or out of favorable alignment with the axis of dilatation!

3. Frontogenesis calculations and time evolution of the fields

In order to show how the vortex circulation influences a scalar field, consider an initial distribution of a scalar quantity Q given by

$$Q(x, y) = -\tanh y. \tag{15}$$

The initial front is oriented along the x-axis, so there is no initial variation of Q with x (Fig. 2). As with the definition of V_T, this Q pattern is implicitly nondimensionalized by some characteristic amplitude for Q-variation. The initial distribution of Q is shown in cross section in Fig. 3, along with its first two derivatives.

Now, given (15) and the results of Section 2, an explicit expression can be found for (5), the frontogenesis. First note that *initially* the angle of inclination (α) between Q isopleths and the x-axis is zero. Thus, by (14),

$$2\gamma \equiv 2\alpha - 2\beta = -2\beta = \frac{\pi}{2} - 2\theta. \tag{16}$$

Since div $\equiv 0$, F can easily be shown to be

$$F = \frac{1}{2}\operatorname{sech}^2 r\left|\left[2\tanh^2 r - \operatorname{sech}^2 r + \frac{\tanh r}{r}\right]\right| \cos\left(\frac{\pi}{2} - 2\theta\right)\Bigg] \operatorname{sech}^2 y. \tag{17}$$

The calculation using (17) is shown in Fig. 4. The pattern fits our intuition nicely—it is antisymmetric about the y-axis. Note that the maximum magnitude for frontogenesis occurs between the radius of maximum wind and the radius of maximum deformation. This is a consequence of the initial conditions and the location of maximum favorability (or unfavorability) of the orientation of the dilatation axes with respect to the maximum frontal gradients.

It is certainly of interest to see how this pattern evolves with time. In principle, this means a solution to the nonlinear advection equation—i.e.,

$$\partial Q/\partial t = -\mathbf{V} \cdot \nabla Q. \tag{18}$$

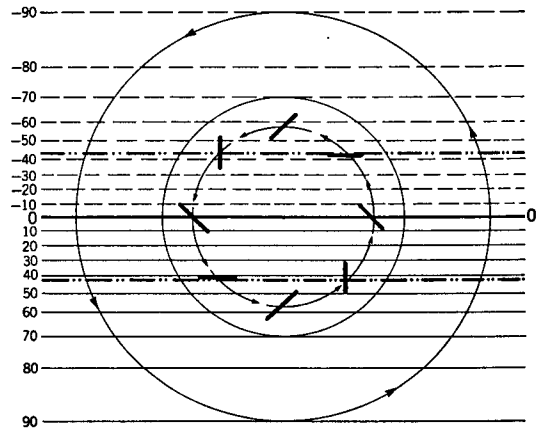

FIG. 2. Schematic plan view of the vortex circulation, showing the initial distribution of the unspecified, nondimensional quantity Q (×100—thin solid and dashed lines). The inner circle is at the radius of maximum winds and the orientation of the resultant deformation's dilatation axes are shown at 45° intervals around that circle. The next circle outward is at the radius of maximum def_R (refer to Fig. 1). The locations of the extrema in $\partial(\partial Q/\partial y)/\partial y$ are indicated by the dashed, double-dotted lines.

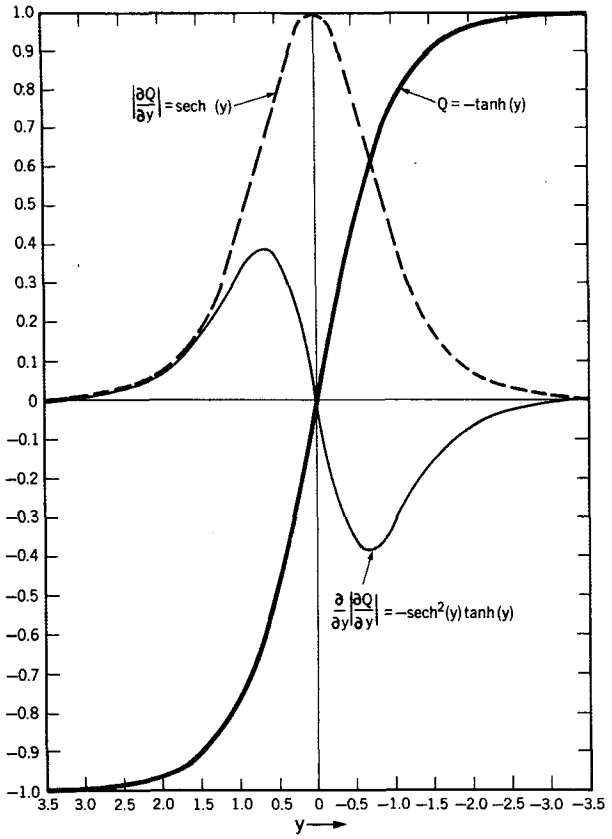

FIG. 3. Cross-sectional (radial) presentation of the Q-field and its first two derivatives at the initial time along the y-axis.

The right hand side of (18) at the initial moment is simply found from

$$-\mathbf{V}\cdot\nabla Q = -(u\partial Q/\partial x + v\partial Q/\partial y),$$

using (10) and (18) and differentiating (15) appropriately. Thus,

$$\partial Q/\partial t|_{t=t_0} = \operatorname{sech}^2 r \tanh r \operatorname{sech}^2 y \cos\theta, \quad (19)$$

where t_0 is the initial time. The field of $\partial Q/\partial t$ at $t = t_0$ is shown in Fig. 5. As one expects, maximum advection is at the radius of maximum winds, along the x-axis.

By introducing the only approximation needed to obtain a solution for (18):

$$Q(x, y, t = t_1) \approx Q(x, y, t = t_0) + (\partial Q/\partial t)|_{t=t_0}\Delta t, \quad (20)$$

the new Q-field can be found. If Δt ($\equiv t_1 - t_0$) in these nondimensional forms is set equal to unity, then (20) becomes [using (19) and (15)]

$$Q(x, y, t = t_1) = -\tanh y + \operatorname{sech}^2 r \tanh r \operatorname{sech}^2 y \cos\theta. \quad (21)$$

A plot of (21) is shown in Fig. 6. This also agrees nicely with our intuition. At first glance, it seems that there is no analytic expression for ∇Q at this point, so there does not appear to be any way to carry this forward any further. Note, however, that

$$\partial(\nabla Q)/\partial t = \nabla(\partial Q/\partial t). \quad (22)$$

Thus, by applying the ∇-operator to (19), $\partial(\nabla Q)/\partial t$ can be found using (22). After much tedious algebra, it can be shown that

$$\begin{aligned}\partial(\nabla Q)/\partial t = \nabla\{&\operatorname{sech}^2 r \tanh r \operatorname{sech}^2 y \cos\theta\}\\ = &\operatorname{sech}^2 r \operatorname{sech}^2 y\{[\cos^2\theta\{\operatorname{sech}^2 r - 2\tanh^2 r\}\\ &+ \sin^2\theta(\tanh r/r)]\mathbf{i} + [\sin\theta\cos\theta\{\operatorname{sech}^2 r\\ &- 2\tanh^2 r - (\tanh r/r)\}\\ &- 2\cos\theta\tanh r\tanh y]\mathbf{j}\}. \quad (23)\end{aligned}$$

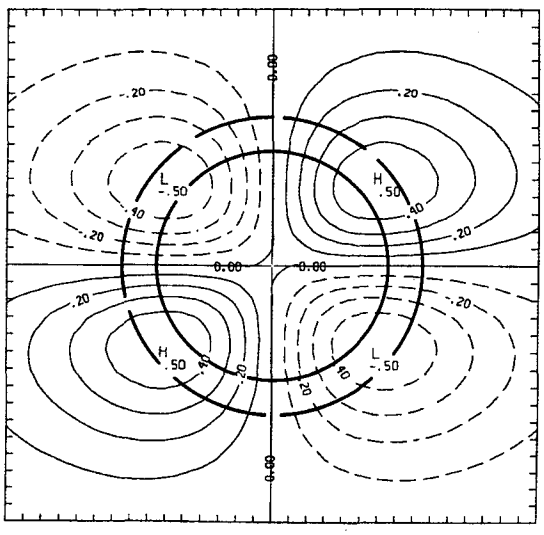

FIG. 4. Initial field (i.e., at $t = t_0$) of the frontogenesis. The solid circle is at the radius of maximum winds, while the dashed circle is at the radius of maximum deformation (about $r = 0.85$).

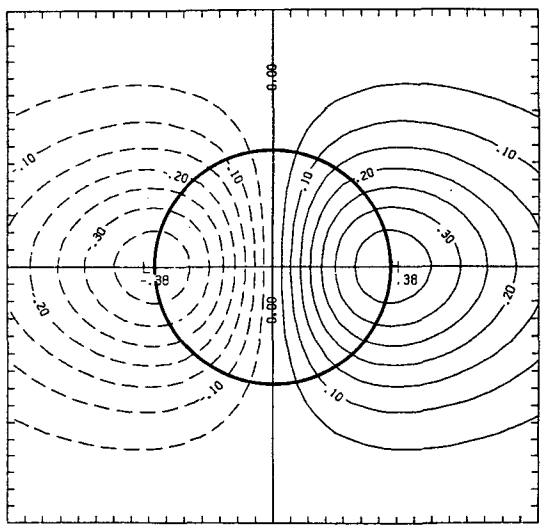

FIG. 5. Initial field of advection, with solid circle at the radius of maximum winds.

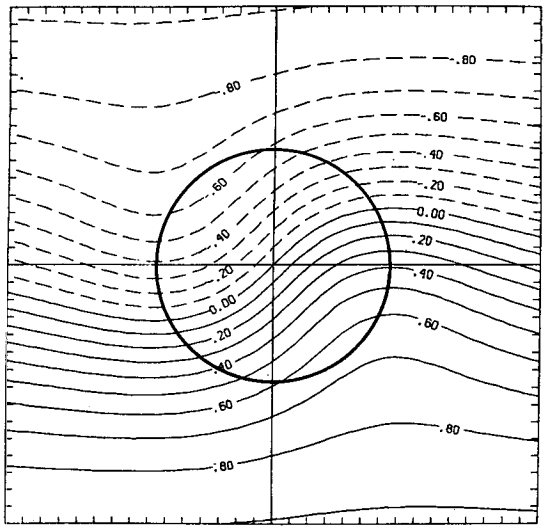

FIG. 6. Field of Q after the first time step (i.e., at $t = t_1$). Solid circle is at radius of maximum winds.

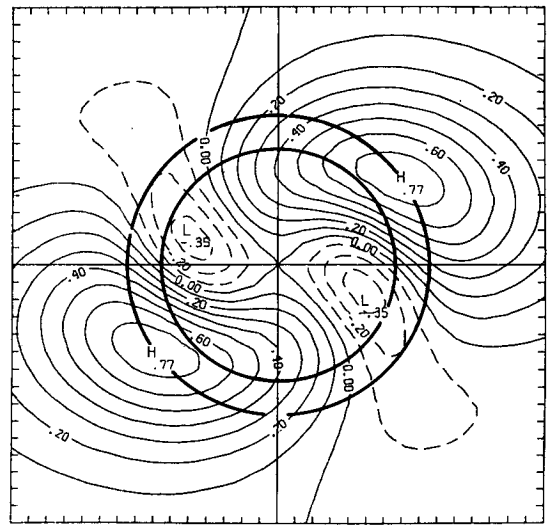

FIG. 8. As in Fig. 4, except at time $t = t_1$.

where **i** and **j** are unit vectors in the x- and y-directions, respectively. As with the Q-field, ∇Q at time $t = t_1$ can be found by saying that

$$\nabla Q(x, y, t = t_1) \approx \nabla Q(x, y, t = t_0) + [\partial(\nabla Q)/\partial t]|_{t=t_0}\Delta t. \quad (24)$$

A plot of $|\nabla Q|$ at time $t = t_1$ is shown in Fig. 7.

Now, armed with the ∇Q-field at the advanced time, the frontogenesis (Fig. 8) can be re-computed from (5), as well as the local time change by advection (Fig. 9). Note the increase of frontogenesis, the decrease of frontolysis, and the position shift of extrema in the field of flow as seen in Fig. 8. Recall that frontogenesis depends on $|\nabla Q|$—in a frontolytic situation, the pattern will be decreasingly frontolytic as the gradient decreases. Further, the peak in frontogenesis shifts with time toward the radius of maximum deformation.

Observe in Fig. 8 that frontogenesis has become positive outside the radius of maximum winds, below the positive x-axis and above the negative x-axis, where it had been negative initially. The equivalent effect does not occur along the y-axis. Since this represents a "propagation" of frontogenesis into the wind field, it deserves explanation. If one examines the relationship of the newly computed Q-field (Fig. 6) to the (time-independent) axes of dilatation (Fig. 2), Q-isopleths are seen to have been rotated by the vortex, to where they are oriented at less than 45° with respect to the axis of dilatation. Thus, frontogenesis has been created

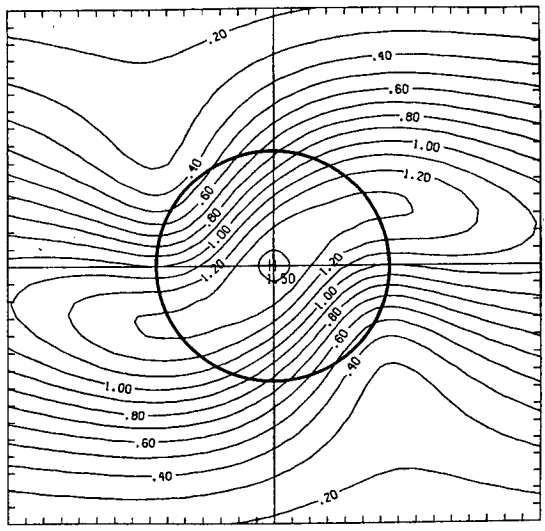

FIG. 7. Field of Q-gradient magnitude at time $t = t_1$, with circle at radius of maximum winds.

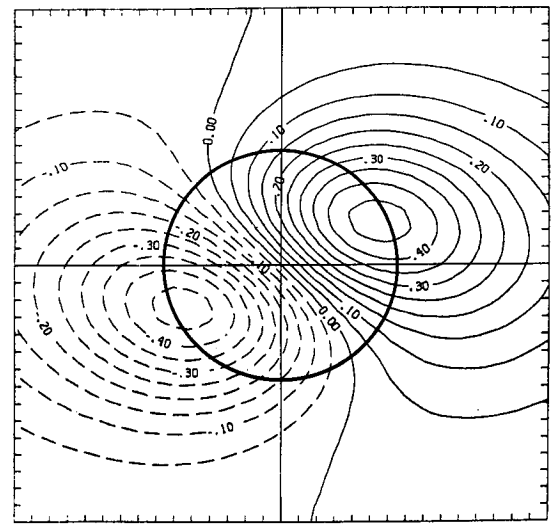

FIG. 9. As in Fig. 5, except at time $t = t_1$.

by rotation in an indirect fashion, as mentioned at the end of Section 2.

In Fig. 9, note that the strongest gradient of $\partial Q/\partial t$ persists at the origin (as in Fig. 5). As suggested by (19) and (22), the gradient should increase most rapidly at the origin. Fig. 7 shows this to be the case. Once again, if the $\partial Q/\partial t$ of Fig. 9 is added to the new Q-field of Fig. 6, the Q-field at time $t = t_2 = t_0 + 2\Delta t$ is obtained, shown in Fig. 10.

In principle, this process can be continued indefinitely. However, applying a ∇-operator to the results of (24) would obviously result in an exceedingly complex expression. This rapidly increasing complexity is a direct result of the nonlinearity of the advection Eq. (17). The solutions obtained are spatially exact, but the time-stepping process [(20) and (24)] is only an approximation. This involves, among other things, another "linearity" assumption, concerned with the time derivative (as opposed to the linearity of a differential equation or of the spatial derivative). Since the difference in the field of Q over two "unit" time steps is rather large (compare Fig. 2 with Fig. 10), the validity of the time linearity assumption is suspect. Nevertheless, the fields' evolution as shown is certainly in agreement with intuition, so the problems with the time derivative approximation are probably not too serious during these early stages.

4. Discussion of results

Perhaps the most important point to be emphasized from all this analytic verification of intuition is that *vorticity has important direct and indirect effects on frontogenesis.* This in spite of its not appearing in the conventional expression for frontogenesis (5). Vorticity's direct effects are through its implicit deformations, in turn resulting from its spatial variations, as discussed in Section 2. Note that the flow in this example is nondivergent, but the concept has broader generality, since only very restrictive types of associated divergence fields could accompany a flow field with spatially-varying vorticity, but without deformation. Observe also that one might just as well say that a spatially-varying *divergence* field contains implicit deformations. The emphasis on vorticity in this paper is motivated by its non-appearance in the conventional definition for frontogenesis (5). Intuitively, spatial differences in vorticity result in different parts of the field experiencing different "rotation rates," causing stretching (deformation) of the scalar field. An indirect effect of vorticity on frontogenesis occurs when the pattern is rotated from an unfavorable relationship with respect to deformation fields to a favorable one (or vice versa).

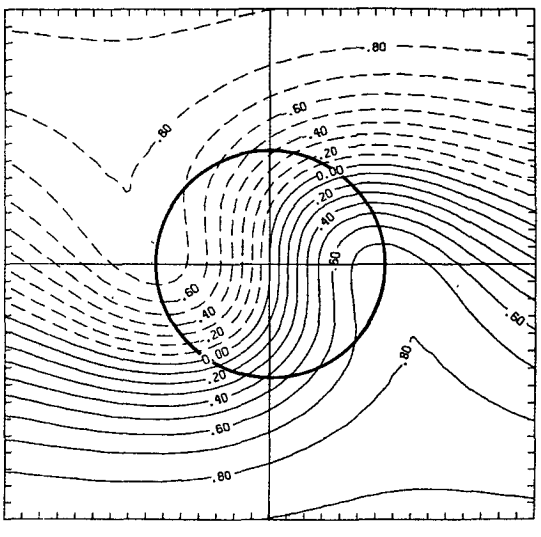

FIG. 10. As in Fig. 6, except at time $t = t_2$.

As an aside to these calculations, it can be seen (e.g., Fig. 10) that the resulting patterns have more than passing resemblance to actual atmospheric frontal zones in a vortex flow regime. The resemblance results from purely *kinematic* relationships of the Q-field to the flow field in a vortex, in spite of the very simple model. Observe in Fig. 10 that the isopleths of Q are coming into alignment everywhere with the axes of dilatation. This has the effect of an inward spiralling frontal pattern even when there is no convergence!

As suggested in Section 1, *scale is not implied anywhere in this model.* Thus, this deduction can be made: when a vortex operates on a simple, initially one-dimensional frontal zone, the result will always look something like Fig. 10 (perhaps modified by the inclusion of divergence). This may be a partial explanation for the remarkable resemblance between an extratropical cyclone and the storm-scale mesocyclone in a supercell thunderstorm (Lemon and Doswell, 1979).

If these results were extended in time, the vortex should wrap the frontal zone around itself many times. As an example of this, consider Fig. 1 in Sykes and Lewellen (1982)—compare Fig. 10 with their Fig. 1a. Presumably, the behavior of the system shown here with time results in a convolution of isopleths in the vortex "core" and accompanying "braided" fronts (as in their Fig. 1b). Another example can be seen in Kessler's (1969) Fig. 3.11, which should be compared with Fig. 6 and Fig. 10. These examples represent *dynamical* rather than purely kinematic processes. However, the dynamics involved produce *kinematic* fields which more than superficially resemble the model in this study, and the behavior of scalar quantities in such a flow is largely determined by those kinematic fields. Clearly, dynamical models allow for feedbacks between the scalar quantities and the flow which are not included in a kinematic approach.

Since the model considered here is not viscous, the process of convolution can go on indefinitely. Naturally, the real atmosphere is more or less viscous, so the strong gradients brought about by this deforma-

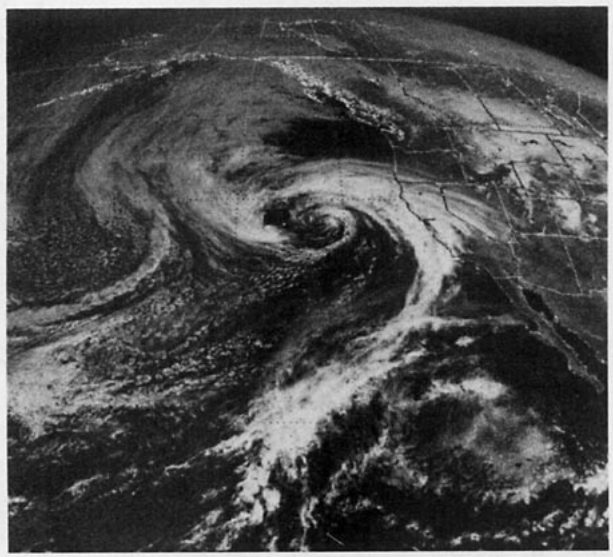

FIG. 11. Visible satellite image of spiraling cloud pattern in eastern Pacific.

tion–frontogenesis should result in locally enhanced mixing, which eventually acts to wipe out these gradients. If an atmospheric vortex is characterized by relatively weak mixing, this convolution should be apparent—see Fig. 11 as an example of what appears to be such a system. Such tightly wound cloud spirals are relatively rare and when they do occur, they are almost always over oceans. One might suspect that mixing may be less under conditions of strong static stability and minimal surface friction (perhaps most common over oceans, at least in the *warm* season), thus enhancing the development of a convoluted cloud spiral in the vortex. One should also note that oceanic cyclones are typically more intense, which might result in greater spatial vorticity variations.

Acknowledgments. The author gained a great deal from discussions on this topic with Drs. S. L. Barnes, J. M. Brown, R. A. Maddox and M. A. Shapiro. Jeannie Sanderson and Elaine Ardourel prepared the manuscript and Mr. J. G. Meitin helped with computer graphics on several of the figures. Also, the manuscript benefitted greatly from comments by Drs. Brown and Barnes, as well as additional careful and thoughtful reviews by the anonymous reviewers (one of whose comments allowed a considerable simplification of Eq. 23).

REFERENCES

Doswell, C. A., III, 1982: Diagnosis of weather events via kinematic analysis. *Preprints Ninth Conf. Weather Forecasting and Analysis,* Seattle, Amer. Meteor. Soc., 300–303.

Kessler, E., 1969: *On the Distribution and Continuity of Water Substance in Atmospheric Circulations. Meteor. Monogr.,* No. 32, Amer. Meteor. Soc., 84 pp.

Lemon, L. R. and C. A. Doswell III, 1979: Severe thunderstorm evolution and mesocyclone structure as related to tornadogenesis. *Mon. Wea. Rev.,* **107,** 1189–1197.

Miller, J. E., 1948: On the concept of frontogenesis. *J. Meteor.,* **5,** 169–171.

Petterssen, S., 1956: *Weather Analysis and Forecasting. Vol. I: Motion and Motion Systems,* 2nd ed., McGraw–Hill, 428 pp.

Saucier, W. J., 1955: *Principles of Meteorological Analysis.* University of Chicago, 438 pp.

Sykes, R. I., and W. S. Lewellen, 1982: A numerical study of breaking Kelvin–Helmholtz billows using a Reynolds-stress turbulence closure model. *J. Atmos. Sci.,* **39,** 1506–1520.

Welander, P., 1955: Studies on the general development of motion in a two-dimensional ideal fluid. *Tellus,* **7,** 141–155.